Chemical bonding in hydrogen and lithium under pressure

Ivan I. Naumov, Russell J. Hemley, Roald Hoffmann, and N. W. Ashcroft

Citation: The Journal of Chemical Physics **143**, 064702 (2015); doi: 10.1063/1.4928076
View online: http://dx.doi.org/10.1063/1.4928076
View Table of Contents: http://scitation.aip.org/content/aip/journal/jcp/143/6?ver=pdfcov
Published by the AIP Publishing

Chemical bonding in hydrogen and lithium under pressure

Ivan I. Naumov,[1] Russell J. Hemley,[1] Roald Hoffmann,[2] and N. W. Ashcroft[3]
[1]*Geophysical Laboratory, Carnegie Institution of Washington, 5251 Broad Branch Rd. NW, Washington, DC 20015, USA*
[2]*Baker Laboratory, Department of Chemistry and Chemical Biology, Cornell University, Ithaca, New York 14853, USA*
[3]*Laboratory of Atomic and Solid State Physics and Cornell Center for Materials Research, Cornell University, Clark Hall, Ithaca, New York 14853, USA*

(Received 2 June 2015; accepted 21 July 2015; published online 12 August 2015)

Though hydrogen and lithium have been assigned a common column of the periodic table, their crystalline states under common conditions are drastically different: the former at temperatures where it is crystalline is a molecular insulator, whereas the latter is a metal that takes on simple structures. On compression, however, the two come to share some structural and other similarities associated with the *insulator-to-metal* and *metal-to-insulator* transitions, respectively. To gain a deeper understanding of differences and parallels in the behaviors of compressed hydrogen and lithium, we performed an *ab initio* comparative study of these systems in selected *identical* structures. Both elements undergo a continuous pressure-induced *s-p* electronic transition, though this is at a much earlier stage of development for H. The valence charge density accumulates in interstitial regions in Li but not in H in structures examined over the same range of compression. Moreover, the valence charge density distributions or electron localization functions for the same arrangement of atoms *mirror* each other as one proceeds from one element to the other. Application of the virial theorem shows that the kinetic and potential energies jump across the first-order phase transitions in H and Li are opposite in sign because of non-local effects in the Li pseudopotential. Finally, the common tendency of compressed H and Li to adopt three-fold coordinated structures as found is explained by the fact that such structures are capable of yielding a profound pseudogap in the electronic densities of states at the Fermi level, thereby reducing the kinetic energy. These results have implications for the phase diagrams of these elements and also for the search for new structures with novel properties. [http://dx.doi.org/10.1063/1.4928076]

I. INTRODUCTION

Hydrogen (H) typically graces the top of Group 1 of the periodic table, yet it is rarely termed an alkali metal.[1,2] Recent high-pressure experiments have put the distinction between H and the lightest alkalis in a new light. New phases of H have been observed experimentally[3–6] and predicted theoretically.[7,8] Though those of H remain molecular over a broad range of $P-T$ conditions,[9] H begins to share structural similarities with Li at certain pressures. H transforms to threefold coordinated layered structures consisting of distorted graphene sheets (200-350 GPa), whereas Li, which has *bcc* and 9*R* structures at low pressures, transforms to threefold coordinated, non-closed packed structures (40-450 GPa).[10–13] In addition, both elements have maxima in their melting curves and exhibit low-temperature melting at megabar (>100 GPa) pressures.[13–19] But most notable actually is a distinction in their electronic transitions, with an *insulator-metal* transition in H versus a *metal-insulator* transition in Li on compression. The conventional view that H undergoes pressure-induced dissociation to form a simple monatomic metallic solid[2] has been replaced by the realization that the material passes through a semiconducting-semimetallic state with complex structures that are far from close-packed.[20] In contrast, starting at low pressure, Li becomes a poorer metal with increasing compression,[21] with a gap opening above 80 GPa, somewhat the reverse of the conventional dogma that all materials must become (or remain) metallic at high pressure. Li re-enters a metallic state above 120 GPa.[27]

As pointed out previously,[22] the Hamiltonians of H and Li are quite similar. Expressed in terms one- and two-particle density operators $\hat{\rho}^{(1)}$ and $\hat{\rho}^{(2)}$, we have for hydrogen,

$$\hat{H} = \hat{T}_{\mathrm{p}} + \hat{T}_{\mathrm{e}} + \frac{1}{2}\int_{\mathrm{V}} \mathrm{d}\mathbf{r} \int_{\mathrm{V}} \mathrm{d}\mathbf{r}'\, \mathrm{v_c}(\mathbf{r}-\mathbf{r}') \times \left\{\hat{\rho}_p^{(2)}(\mathbf{r},\mathbf{r}') - 2\hat{\rho}_p^{(1)}(\mathbf{r})\hat{\rho}_e^{(1)}(\mathbf{r}') + \hat{\rho}_e^{(2)}(\mathbf{r},\mathbf{r}')\right\}, \quad (1)$$

while for lithium,

$$\hat{H} = \hat{T}_{\mathrm{n}} + \hat{T}_{\mathrm{e}} + \frac{1}{2}\int_{\mathrm{V}} \mathrm{d}\mathbf{r} \int_{\mathrm{V}} \mathrm{d}\mathbf{r}'\, \mathrm{v_c}(\mathbf{r}-\mathbf{r}') \times \left\{9\hat{\rho}_n^{(2)}(\mathbf{r},\mathbf{r}') - 6\hat{\rho}_n^{(1)}(\mathbf{r})\hat{\rho}_e^{(1)}(\mathbf{r}') + \hat{\rho}_e^{(2)}(\mathbf{r},\mathbf{r}')\right\}, \quad (2)$$

where the indices p and n are used to distinguish between the proton and Li nuclei, the $\hat{T}$ are kinetic energy operators for the electrons and nuclei, and $\mathrm{v_c}(\mathbf{r}-\mathbf{r}') = \mathrm{e}/|\mathbf{r}-\mathbf{r}'|$ is the fundamental Coulomb interaction. The conventional light metals, Li and Na, are, as noted, textbook examples of simplest *s*-metals—at normal pressure and room temperature, they all crystallize in the *bcc* structure and are described well in the nearly free-electron (NFE) approximation by using

perturbation techniques up to the second order in a weak pseudopotential.[23–25] Naively, one can expect them to remain highly coordinated metals and become even more free-electron-like as pressure increases. However, when compressed, they undergo a number of phase transitions, first to *fcc* and then to more complex structures with relatively low symmetry and coordination numbers and, what is more unexpected, become less conductive and even insulating. Li, for example, undergoes a metal-semiconductor transition at 80 GPa[26] prior to re-entering a metallic phase,[27] whereas Na becomes optically transparent above 180 GPa.[28]

Exotic and often counterintuitive behavior of these and heavier alkali metals under pressure has received intense attention in the last decade (e.g., Refs. 21 and 29–35). A notably interesting feature of high-pressure phases of the alkalis is the tendency toward interstitial localization of charge which resembles that seen in the unusual class of materials called electrides.[10,11,21,35–42] Classical electrides are complex organic and, as a rule, non-metallic compounds in which some electrons occupy interstitial regions or cavities rather than residing on the alkali-metal nucleus or near them.[43–46] Neaton and Ashcroft[21] were the first to show that this type of localization can be induced in elemental metals under pressure. Using first-principles pseudopotential calculations, they predicted that above 100 GPa, Li adopts a semimetallic low-coordinated "paired" *Cmca*-4 phase with charge density peaking in the interstitial regions, loosely analogous to organic electrides.[46] Later, similar behavior of valence electron distributions was found in a number of experimentally observed phases realized in Li (*bcc*,[47] *cI*16,[39] *oC*88, *o*C40, *o*C24[41]), Na (hP4[26]), and Cs (Cs-IV[42] and Cs-V [38]). The descriptions of the interstitial charge density-maxima form are presented in Refs. 21, 35, 38, 40, 46, 48, and 49 and are examined further in detail in Ref. 50.

Here, we re-examine the above phenomena by considering selected prototype structures for the lightest alkalis, H and Li. The *Cmca*-4 structure is among the lowest energy phases considered for Li,[21] and it has also been well-studied as a high-pressure structure for hydrogen.[51] This structure has four atoms per primitive unit cell (or 16 atoms per conventional unit cell) and can be *continuously* derived from the *fcc* by introducing a Peierls-like distortion that doubles the lattice parameter along the [001] direction but is also accompanied by a strong homogeneous deformation. We also examine selected other structures for H and Li, including those both experimentally established and predicted previously by theory.

Our analysis reveals parallels between H and Li that can be understood in terms of pressure-induced changes in the associated electronic structures and bonding of the two elements under pressure. Whereas in Li, the *s-p* hybridization is already well underway at 1 bar; in H, such hybridization takes place only at elevated compressions—H behaves as a high pressure version of Li. All common structures exhibit distinct valence charge densities and/or electron localization functions (ELFs) that mirror each other. Using the virial theorem, we demonstrate that first-order pressure-induced phase transitions in H and Li are accompanied by discontinuous jumps in kinetic energy that are opposite as a result of orthogonality. We also show that both compressed H and Li tend to adopt three-fold coordinated structures capable of forming a pronounced pseudogap (if not a real bandgap) at the Fermi level in the density of states (DOS). The results also reveal parallels to predictions of important early generalized valence bond calculations of metallic bonding in atomic clusters.[55,56] Analyses of the results provide a unifying picture for the electronic, bonding, and structural properties of the light alkali metals.

II. THEORETICAL METHODS

At a one-electron level, both solid H and Li can be accurately described by using pseudopotentials. Though the H atom lacks core electrons, it is possible to generate a pseudopotential such that it is soft and has no bound states (as for any other atom). Such a pseudopotential allows the use of softer wave functions that reach convergent results faster. Removing the cusp of the 1/r potential has only a slight effect on properties such as the electronic spectrum and total energy,[53] as discussed further below. Our calculations were performed using norm-conserving pseudopotentials and the all-electron projector augmented wave (PAW) method as implemented in the ABINIT package. PAW atomic data and norm-conserving pseudopotentials were generated with ATOMPAW and OPIUM codes using Perdew-Burke-Ernzerhof GGA functional. In the case of norm-conserving pseudopotentials, the cutoff radius r_c has been chosen to be 0.5 and 1.25 bohrs for H and Li, respectively; this radius is less than 1/2 of the shortest interatomic distance in the target calculations. Use of pseudopotentials along with a more accurate PAW formalism allowed separation valence and core electrons in order to explicitly evaluate how their behavior is effected by the orthogonal effects imposed by the cores. The pseudopotential calculations were tested against the PAW calculations, and very good consistency between the two was found. A cutoff energy of 100 Ry was used for the plane-wave expansion of the valence and conduction band wave functions. A $20 \times 20 \times 20$ Monkhorst-Pack **k**-point grid has been used in the case of three-dimensional structures and a $20 \times 20 \times 1$ grid in the case of graphene lattice.

We exploit the virial theorem, which in the framework of the local-density approximation (LDA) pseudopotential theory can be expressed by the following relation between the pressure P, total energy E_{tot}, and kinetic energy E_{kin} of the system:[52,54]

$$E_{tot} = -E_{kin} + 3PV + \int \rho(\mathbf{r})(4\varepsilon_{xc} - 3\mu_{xc})d\mathbf{r} + \sum_{i,\,\mu} \int \psi_i^*(\mathbf{r}) \sum_l \left[\frac{d(r'V_{\mu,l}(r'))}{dr'} \hat{P}_l \right]_{\mathbf{r}'=r-R_\mu} \psi_i(\mathbf{r})d\mathbf{r}, \quad (3)$$

where V = ΩN is the volume of the system, ρ(**r**) the valence charge density, ε_{xc} the exchange-correlation energy density, μ_{xc} the exchange-correlation potential, $\psi_i(\mathbf{r})$ the wave function of the occupied state i, $V_{\mu,l}$ the unscreened pseudopotentials, $\hat{P}_l$ the angular momentum operator, and $\mathbf{R}_\mu$ the position of atom μ. Expression (3) immediately allows one to write the following expression for the enthalpy $H = E_{tot} + PV$:

$$H = -E_{kin} + 4PV + \int \rho(\mathbf{r})(4\varepsilon_{xc} - 3\mu_{xc})d\mathbf{r} + \sum_{i,\,\mu} \int \psi_i^*(\mathbf{r}) \sum_l \left[\frac{d(r'V_{\mu,l}(r'))}{dr'} \hat{P}_l \right]_{\mathbf{r}'=r-R_\mu} \psi_i(\mathbf{r})d\mathbf{r}. \quad (4)$$

It should be noted that for the nuclear $1/r$ potential, the last term on the right hand side (rhs) of Eq. (4) is identically zero. When the real potential $1/r$ at the origin is replaced by a set of norm conserving pseudopotentials V_l, this term becomes finite and usually negative. In the case for H, however, it is relatively small because the main component ($V_{l=0}$) of the pseudopotential is hard and imitates well the original $1/r$ potential attributed to an absence of any core states. In contrast, in Li, the $2s$ electrons see a cancelled (pseudo)potential because there are core states ($1s$) with the same angular momentum. At the same time, the $2p$ electrons see an almost full potential because there are no p core states with which they would be required to be orthogonal.

III. RESULTS AND DISCUSSION

A. Electronic structure overview

The core configuration for Li [$1s^2$] leads to a small energetic separation between the $2s$ and $2p$ states: the $2s$ electrons lie somewhat lower in energy because they penetrate the inner $1s$ shielding shell deeper than $2p$ (Fig. 1). When a Li atom is placed in a helium cavity mimicking the external pressure, both its $2s$ and $2p$ levels rise with external pressure. But the $2s$ level goes up more steeply, so that $2p$ falls below $2s$.[35] This tendency is retained in going from the confined atoms to compressed bulk materials. As a result, pressure-induced changes in electronic and structural properties in Li have been attributed to an s-p transition in electron density.[29,34] The $2p$ and $2s$ orbitals hybridize, leading to a (pseudo)gap at the Fermi level and accumulation of the electrons in interstitial voids.[21,40,55,56] The $2s$-$2p$ transition in Li is analogous to the electronic transitions in other alkali metals, for example, Na where the strong localization of valence electrons in the interstices is attributed to s-p (-d) hybridization.[50]

In contrast, a hydrogen atom has no core electrons, and the separation in energy between the frontier orbital ($1s$) and higher-energy orbitals ($2s$, $2p$ . . .) is relatively large (Fig. 1). This has led to the view that no s-p transition takes place in hydrogen under pressure.[29] Even though the atomic $2p$ level is significantly higher than the $1s$ level (by ~10 eV), in solid structures under pressure, the conduction $2p$ band moves to lower energy and mixes strongly with the valence $1s$ band, playing a role in the process of pressure-induced metallization. In contrast to H, in Li, the valence electrons localize in the interstitial regions where the crystal potential *is maximal*, a property that is structure-independent, as we show below.

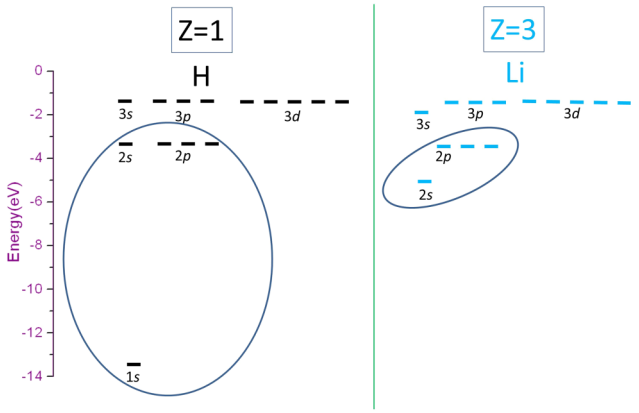

FIG. 1. Energy level diagram for isolated H and Li atoms. The valence and next higher energy levels are circled.

B. Model *fcc* structure

Figure 2 shows the energy band structure, electronic DOS, and 2D electron localization function distribution in a (110) plane for H in model *fcc* structure as a function of compression. In all cases, the Fermi surface does not contact the {111} Brillouin-zone planes, i.e., the Fermi level is lower than the energy level at the L point. Moreover, with increasing pressure, the Fermi surface becomes progressively more spherical and the occupied bandwidth ΔE dramatically increases by a factor of 2.8 as the lattice parameter a decreases from 5 to 3 bohrs (Table I). With a high degree of precision, the bandwidth scales as $1/a^2$, in other words fits the free-electron prediction. Though the occupied band is mainly of $1s$ character, a gradual transfer from s to p orbitals takes place, as seen from the orbital by orbital contributions to the DOS. The ELF exhibits global minima at the octahedral sites located in the middle of the main body diagonals, exactly at the points where the crystal potential shows global maxima. It is worth noticing that the lowest partly occupied single-sheet energy band is split from the rest of the band structure (this is not the case for *fcc*-Li).

The situation changes considerably in passing from H to Li (Fig. 3). The lattice parameters are chosen such that they correspond to three different relationships of the Fermi surface to the {111} planes: (i) just before touching, (ii) at the point of touching, and (iii) after contact. The latter coincides with the passing of the Fermi level through the L point and giving rise to a Van Hove singularity. In contrast to the behavior of H, now the states around the Fermi level for Li are mostly of p-character, even in expanded lattices corresponding to an effective negative pressure. Under applied pressure, the p-component further increases, a process that is accompanied by widening of the gap at L (see also Ref. 21). The latter can be easily understood if one notices that the singly degenerate state at Γ and the second lowest energy state at L are pure $2s$ states (panels (a), (d), and (g)), but the lowest-energy state at L is a pure $2p$ state. Therefore, a wide s-p hybridization gap opens at L. This, however, does not lead to a noticeable minimum in the DOS at the Fermi level. Interestingly, an extremely deep minimum does develop but at a higher energy corresponding to an effective filling of 2 electrons. This situation has parallels that of Be, where strong s-p hybridization leads to a pronounced pseudogap at the Fermi level.[57]

Notably, the occupied bandwidth in *fcc*-Li scales closely with the inverse of the lattice parameter, i.e., $1/a$ in contrast to $1/a^2$ found for hydrogen (Table I). To understand this difference, suppose for a moment that both H and Li are nearly free-electron systems. As such their lowest energy bands E(**k**) can be described by only two parameters V_{111} and V_{200}, the Fourier components of the atomic (pseudo)potentials corresponding to the shortest reciprocal vectors $\mathbf{G}_{111}$ and $\mathbf{G}_{200}$. These components can be easily extracted from Figs. 2 and 3 by inspecting the splitting of the energy levels at the W and K ≡ U

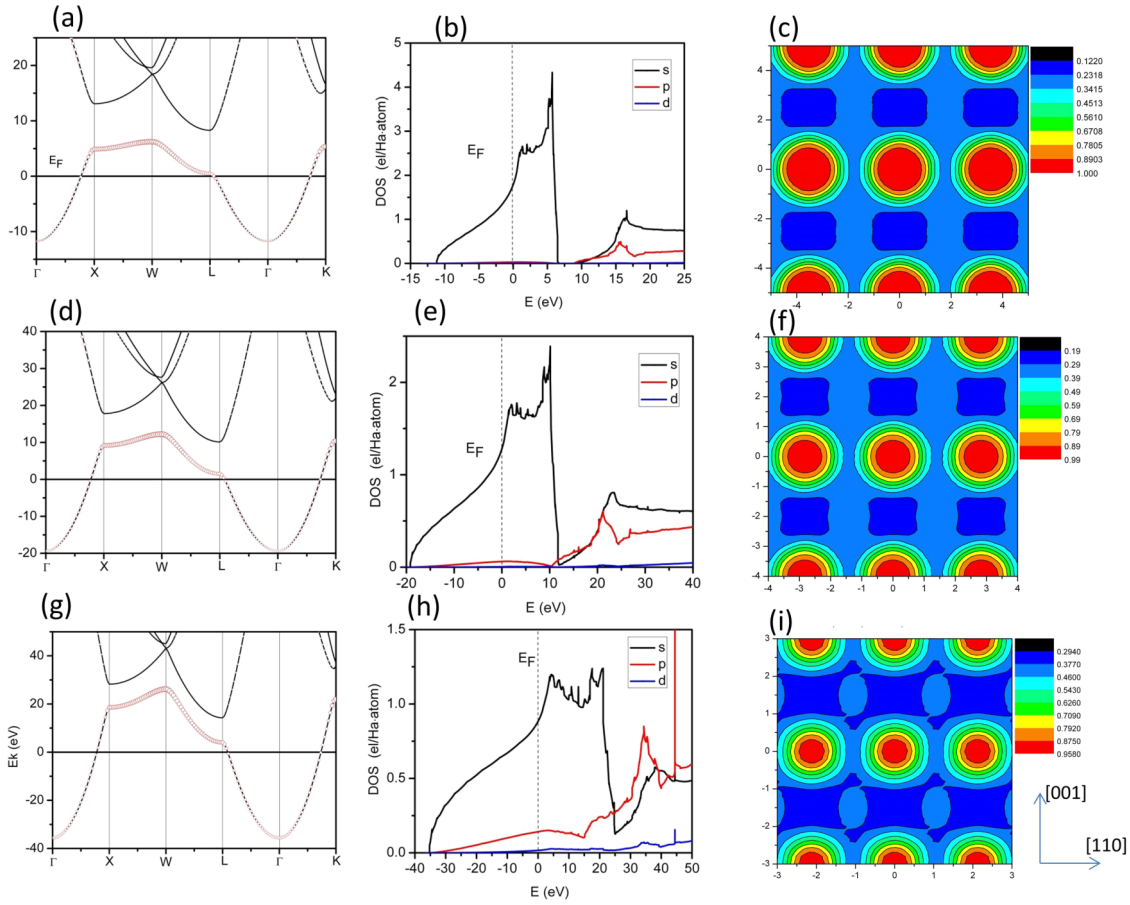

FIG. 2. Calculated static lattice band structure, density of states per electron (DOS), and electron localization function (ELF) values for H in the fcc phase corresponding to three different lattices parameters a and pressures P: ((a)–(c)) $a = 5$ bohrs, $P = -2.4$ GPa. ((d)–(f)) $a = 4$ bohrs, $P = 31.4$ GPa, and ((g)–(i)) $a = 3$ bohrs, $P = 647$ GPa. In (a), (d), and (g), the size of red circles is proportional to the $1s$ character of the wave functions. In (c), (f), and (i), the ions are centered in the red regions; the ordinate points are along [001] and the abscissa is along [110].

points, as discussed in Ref. 58. Table I presents the components V_{111} and V_{200} found in such a way that they reproduce the energy splitting at W exactly and only approximately (but still reasonably well) at K.

One can see that both V_{111} and V_{200} are negative in H, while they are positive in Li. Moreover, when measured relative to the bandwidth ΔE, they progressively decrease with the lattice parameter a in H; the situation is opposite in Li where, for example, $V_{200}/\Delta E$ at $a = 6$ bohrs is as large as 1.01. These results are fully consistent with the fact that the Fermi surface "sphericalizes" in H but elongates and touches the {111} Brillouin faces in Li as the systems are compressed.

TABLE I. Fourier components of the atomic pseudopotentials V and bandwidths ΔE (in eV) for *fcc* H and Li at different lattice parameters (bohrs).

System	Hydrogen			Lithium		
a	3	4	5	6	8	10
V_{111}	−4.73	−3.85	−3.34	3.27	1.17	0.77
V_{200}	−3.77	−3.13	−2.78	3.93	1.63	1.12
ΔE	35.57	19.35	11.75	3.90	3.65	2.73
$V_{111}/\Delta E$	−0.13	−0.20	−0.28	0.84	0.32	0.28
$V_{200}/\Delta E$	−0.10	−0.16	−0.24	1.01	0.45	0.41

This leads to the interesting observation that within the *fcc* structure, it is the H that behaves as a nearly free electron system but not Li. We also point out that the pseudopotential components used here for Li are consistent with the simple single-parameter Ashcroft model pseudopotential determined from the resistivity of liquid Li ($R_{core} = 2.00$ bohrs).[59] This model pseudopotential predicts that the V_{110} component in stress-free *bcc* Li is 1.08 eV.[59] Since at the same pressure, the amplitude $|\mathbf{G}_{110}|$ in *bcc* structure is very close to the amplitude $|\mathbf{G}_{111}|$ in *fcc* structure, the component V_{110} should be compared with ours V_{111} at $a = 8$ (Table I). The latter is 1.17 eV and does coincide well with the former.

In Li, for all values of the lattice parameters explored, the valence electrons tend to avoid the ions and concentrate in the interstitial regions, as seen from the panels (c), (f), and (i), consistent with Refs. 21, 55, and 56. The ELF and corresponding charge densities, however, behave differently. At $a = 10$ or before the contact between the Fermi surface and Brillouin zone, the ELF spreads essentially uniformly throughout the interstitial region (panel (c)). In contrast, after the contact, strong modulations of the ELF form first channel structures ($a = 8$) and then pronounced maxima ($a = 6$), again at the octahedral sites. Roughly, this result can be explained by treating the bandgap at a single Brillouin plane (111) and its symmetry related equivalents in the NFE approximation.[23–25] In

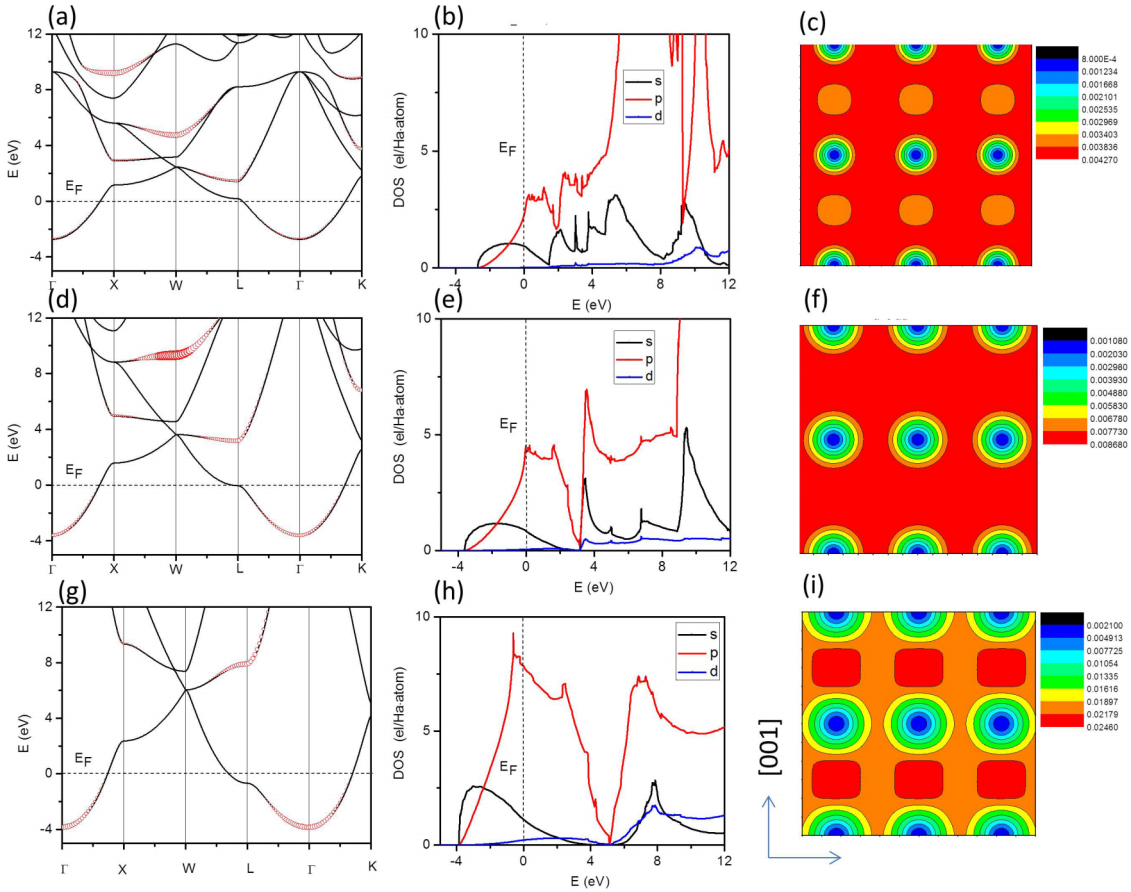

FIG. 3. Same as in Fig. 2, but for Li and 2*s* electrons: ((a)–(c)) $a = 10$ bohrs, $P = -3.1$ GPa. ((d)–(f)) $a = 8$ bohrs, $P = 0.8$ GPa, and ((g)–(i)) $a = 6$ bohrs, $P = 60.4$ GPa. In (a), (d), and (g), the size of red circles is proportional to the 2*s* character of the wave functions. In (c), (f), and (i), the ions are centered in the blue regions.

this approximation, the bandgap under consideration is due to Bragg reflection of electrons, its magnitude $2|\langle \mathbf{k}|V_{ps}|\mathbf{k} - \mathbf{G}_{111}\rangle|$ being given by the scattering matrix element for electrons from $\mathbf{k}$ to $\mathbf{k}$ - $\mathbf{G}_{111}$ (note that $|\langle \mathbf{k}|V_{ps}|\mathbf{k} - \mathbf{G}_{111}\rangle|$ is nothing but the component V_{111} introduced above). For electrons having nearly the Fermi energy, $\mathbf{k} \sim \mathbf{G}_{111}/2$ so that $\mathbf{k}$ - $\mathbf{G}_{111} \sim -\mathbf{G}_{111}/2$. A mixing of electronic states $\mathbf{G}_{111}/2$ and $-\mathbf{G}_{111}/2$ results in the formation of standing waves with a momentum close to the Fermi wave number, i.e., either $\psi = \sin(\mathbf{G}_{111}\cdot\mathbf{r}/2)$ or $\psi = \cos(\mathbf{G}_{111}\cdot\mathbf{r}/2)$. In our particular case, only the first solution is realized because $V_{111} > 0$ and the states near the bottom of the gap (or near the L point) are purely *p*-like; this corresponds to the pile up of charge between the atoms and formation of "*s*-*p* hybridized bonds."[23–25]

We emphasize that the touching of zone faces by the Fermi surface is a *necessary* but not *sufficient* condition for developing charge in the interstitial regions. To illustrate this, we added 0.5 valence electrons to *fcc* H and treated this system as charged in order to force the Fermi surface to be in contact with the {111} planes. Such an artificial inducing of the contact does not move the electrons to the interstitials but rather subtracts the charge from them. Within the NFE approximation, this effect can be explained by the negative value of $|\mathbf{k}|V_{ps}|\mathbf{k} - \mathbf{G}_{111}|$, leading to the *s*-like *antibonding* state, $\psi = \cos(\mathbf{G}_{111}\cdot\mathbf{r}/2)$, at the bottom of the bandgap or in the vicinity of the point L.[23–25] Moreover, comparison of the three-dimensional distributions of ELF in H and Li on compression shows that non-nuclear maxima form only in Li (Fig. 3), in agreement with Figs. 2 and 3. Analysis reveals that these maxima and corresponding peaks in the charge density are located in the regions of *potential minima*. These results also reveal that Li develops an electride-like state already in the closed-packed *fcc* structure, as seen by the connected network of channels directed along [110] consistent with Fig. 4. We point out that interstitial localization of electrons was found in pioneering valence bond calculations for Li rings, planar closed-packed clusters, three-dimensional clusters,[55,56] and Li infinite one-dimensional chains.[60] Indeed, these calculations predicted atom-centered localization of the electrons that suddenly moves to an interstice as the interatomic distance decreases.[60] The electronic localization found in these calculations led to an antiferromagnetic state with spin alternation between adjacent bonds or atoms.

It is interesting that on further compression, the L(2*p*) level drops below the Γ (2s) level; according to LDA-LCGTO calculations, this happens at a pressure of approximately 370 GPa ($\Omega/\Omega_0 = 0.20$).[61] At this critical pressure, the energy band along the Γ-L line becomes extremely flat, raising DOS in the vicinity of the Fermi level. This regime can be also viewed as a point of accidental degeneracy between 2*s* and 2*p* orbitals; such a degeneracy always exists in hydrogen due to pure Coulomb ionic potential acting on an electron. The drop in the 2*p* level below 2*s* with pressure can be explained as follows. The 2*p* orbitals have no nodes in their radial wave functions,

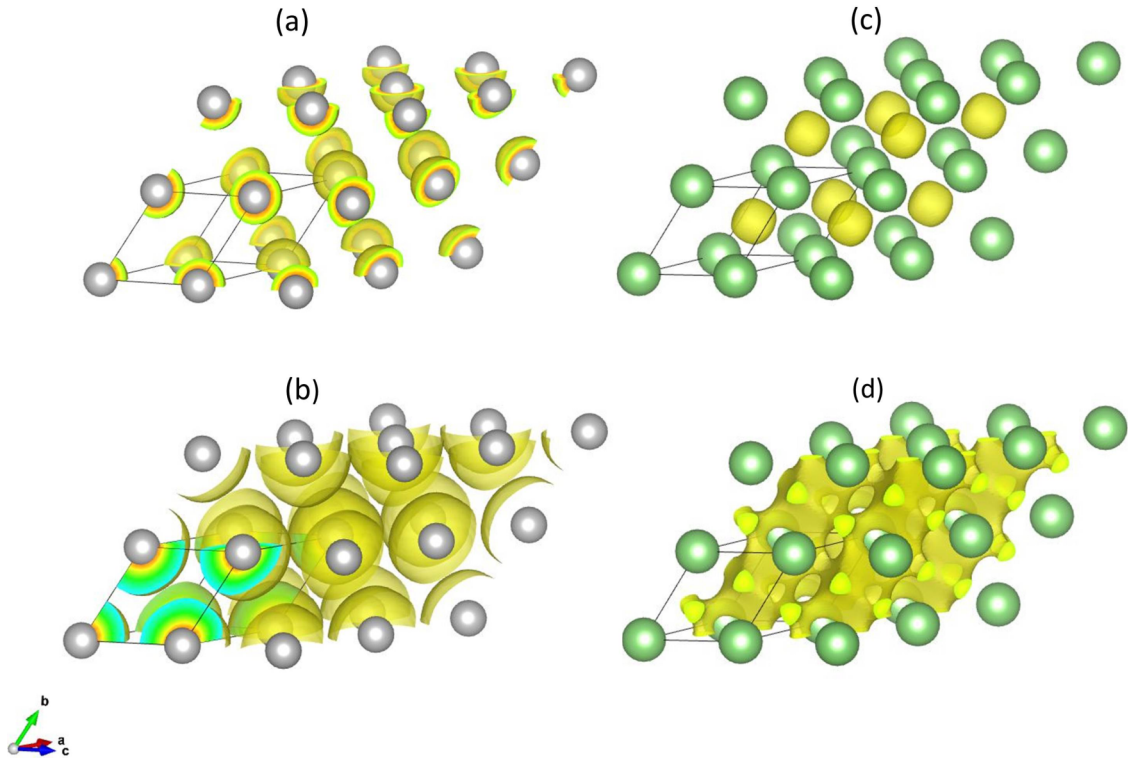

FIG. 4. Isosurfaces of electron localization function (ELF) values for H ((a) and (b)) and Li ((c) and (d)) in the fcc structure which is represented by a 2×2×2 primitive unit cell: ((a) and (b)) $a = 3$ bohrs, isosurfaces = 0.7 and 0.45, respectively. ((c) and (d)) $a = 6$ bohrs, isosurfaces = 0.8 and 0.6, respectively.

whereas the 2*s* counterpart has one. As a result, the 2*p* orbitals are favored on compression because their kinetic energy rises less steeply than that for 2*s*. Another way of reaching this conclusion derives from the fact that the 2*s* orbital always has a larger density far away from nucleus and is therefore more destabilized relative to 2*p* with pressure.

C. *Cmca*-4 structure

In passing from *fcc* to *Cmca*-4, the electronic properties of H and Li change dramatically (Figs. 5 and 6). The major change is the formation of a pronounced pseudogap at the Fermi level in the DOS (panels (b) and (d) in Fig. 6), especially in Li. As in the *fcc* structure, the valence bands in Li are significantly flatter and their widths are noticeably narrower than those in H. Moreover, their topological features and orbital compositions are also principally different. Consider, for example, the Γ-U-Y line (Fig. 5) along which the electronic spectrum exhibits a (semi)metallic behavior, as discussed in Refs. 21 and 51. In the vicinity of U, all the four lowest-energy levels in H have (1)*s*-character, but only the third level is (2)*s*-derived in Li. At the Γ point, the third energy level in H is the bottom of the bonding $2p_z$ band, which crosses the Fermi level at pressures above 300 GPa leading to a new and more electronically conductive semimetallic state. In contrast, this bottom of the band in Li is the second level, which is already well below the E_F at a pressure of 77 GPa.

Figures 5 and 6 show that the band structures of *Cmca*-4 type H and Li are close to those of a zero-bandgap semiconductor. The band structures are characterized by several crossings of two different levels near the E_F. Such crossings, however, take place at different **k**-points in the two elements. In H, for example, one appears between and Γ and Y; in contrast, Li exhibits no crossing along Γ-Y, but instead has one between Γ and S. Naively, one might assume that only different types of Peierls-like distortions could induce a real gap in the comparable counterparts.

In reality, however, a fully gapped semiconducting state appears in both materials via the sliding of alternate layers towards the polar $Cmc2_1$ structure.[20,21,62] This means that the contact lines between the conduction and valence bands in *Cmca*-4 phases of H and Li are protected by inversion symmetry, as discussed in Ref. 20.

The imposed structural similarity between H and Li thus reveals important differences in their electronic structures. These differences are especially clear from the charge density distributions (Fig. 7). Perhaps the most striking observation is the inverted electron density distributions on H and Li: the maxima (minima) in H correspond directly to the minima (maxima) in Li. For the latter, the electron density maxima in the interstitial regions arise from σ *s*-*p* and π *p*-*p* bondings within each buckled layer parallel to the *xy* plane. Inverting the electron charge density within the same system with one valence electron can be formally described by the operation $\rho(\mathbf{r}) \rightarrow 2e/\Omega - \rho(\mathbf{r})$, where Ω is the atomic volume. It is straightforward to show that such an operation leaves invariant both Madelung and Hartree energies associated with the Coulomb interactions between the ions and electrons [Z-Z, Z-ρ(**r**) and ρ(**r**)-ρ(**r**)]. Moreover, in passing from *fcc* to *Cmca*-4 for Li, the kinetic energy *increases* instead of *decreasing*. As discussed below, this change is the reverse of what is typically understood for pressure-induced transitions.

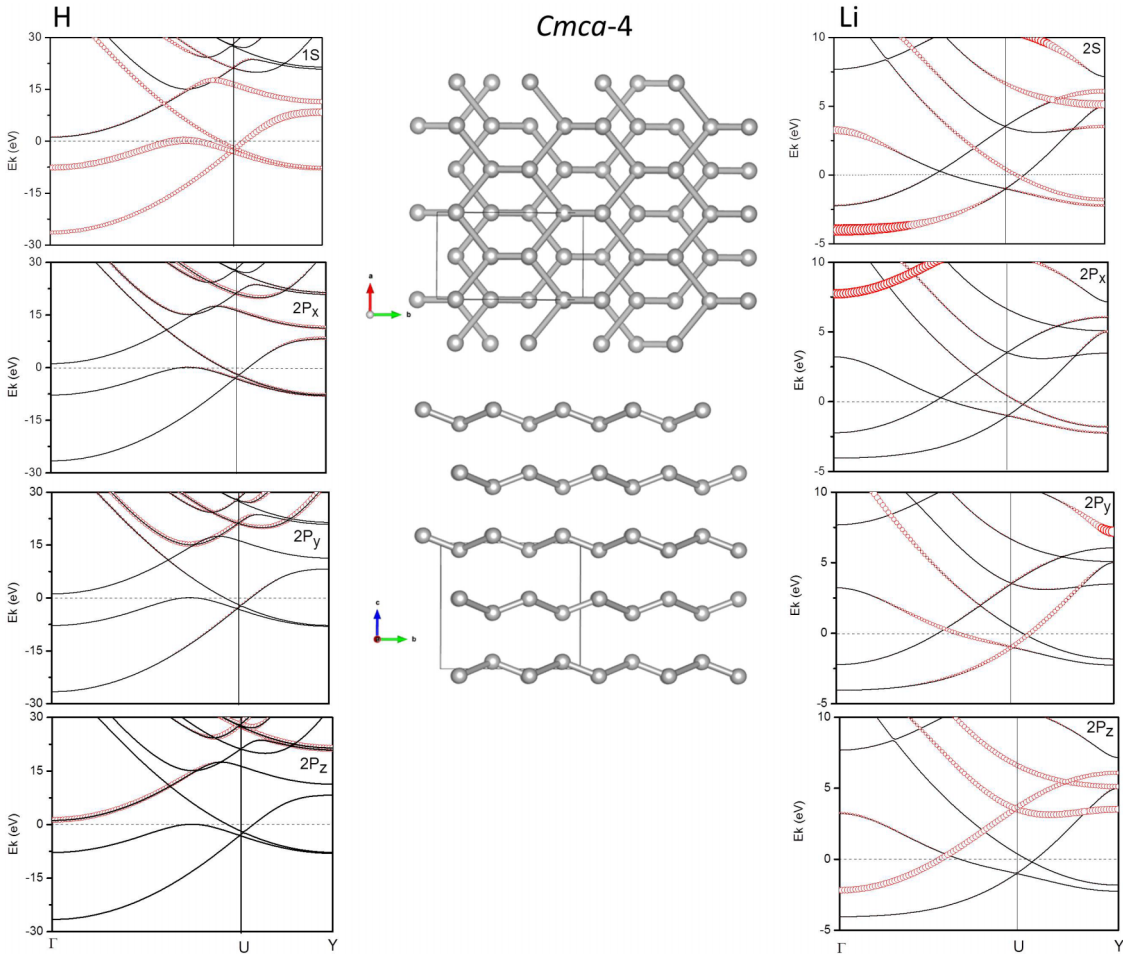

FIG. 5. Static lattice band structures of H (left) and Li (right) in the orthorhombic *Cmca*-4 structure shown in the center. In the case of H, this structure was fully relaxed at 300 GPa, which corresponds to $\Omega = 9.74$ bohrs^3. For the sake of comparison, the same structure was assigned to Li except that the lattice parameters were rescaled to make Ω to be 44.60 bohrs^3; such a rescaling corresponds to a pressure of 77 GPa. All the energies are measured with respect to the Fermi level E_F. The character of the wave functions, which is proportional to the size of red circles, is shown.

The fact that the *fcc* and *Cmca*-4 structures can be *continuously* transformed between each other reveals how the charge density evolves between high- and low-symmetry structures. For this, we consider 4 different points on the continuous pathway: (i) the *Cmca*-4 structure with $\Omega = 113.10$ bohrs^3 where the reduced atomic coordinates however were fixed to those with $\Omega = 33.51$, corresponding to 130 GPa; (ii) the structure obtained from that by relaxing forces; (iii) that obtained from partial relaxing *both* forces and stresses, and (iv) that obtained from (iii) by full relaxation to give the final structure, which is actually *fcc*. As seen from Fig. 8, at stage (i), there are no density maxima in interstitial regions, despite the fact that the structure is paired. It is remarkable that such maxima appear for (ii); these maxima then merge together for (iii) to form zig-zag shaped channels, and then the latter disappear in the final *fcc* structure. We conclude that moving along the *Cmca*-4 → *fcc* pathway *is* not smooth from electronic point of view but involves formation of intermediate charge density waves, even at pressures close to 1 bar.

The energetics of these transitions can be examined using the virial theorem (Table II). Between 130 and 300 GPa, the *Cmca*-4 structure is enthalpically more favorable than the *fcc* phase in H and Li. In passing from *fcc* to *Cmca*-4 in Li, there is an increase in kinetic energy, which is counterintuitive but can be understood by examining the expression for the enthalpy (Eq. (4)). Let P_c be a critical pressure of first-order phase transition at which two phases 1 and 2 are in equilibrium and therefore have the same enthalpy: $H_1 = H_2$. Let phase 2 be a high-pressure phase, then $V_2 < V_1$ and the second term, $4PV$, on rhs of Eq. (4) must suffer a jump down across the $1 \rightarrow 2$ transition. The sum of all the other terms on rhs should undergo a jump up in order to keep the equality $H_1 = H_2$. In the case of the *fcc* → *Cmca*-4 transformation in Li, such a jump is solely due to the last ("pseudopotential") term because the changes in the *minus* kinetic energy and exchange-correlation term behave similar to $P\Delta V$. The critical last term can be actually further decomposed into two parts associated with the operators $V_{\mu,l}(r)\hat{P}_l$ and $\frac{\mathrm{r}dV_{\mu,l}(r)}{dr}\hat{P}_l \equiv -\mathrm{r}F_{\mu,l}(r)\hat{P}$, where in classical terms, the latter would describe the work done on an electron with angular momentum by the nucleus μ. In quantum terms, its expectation value describes the corresponding energy that is transferred to the electron. Analysis shows that this work must jump abruptly across the transition in order to preserve the equality $H_1 = H_2$. We conclude that it is the increased attraction between the $2p$ electrons and Li ions that triggers the *fcc* to *Cmca*-4 structural transition. This

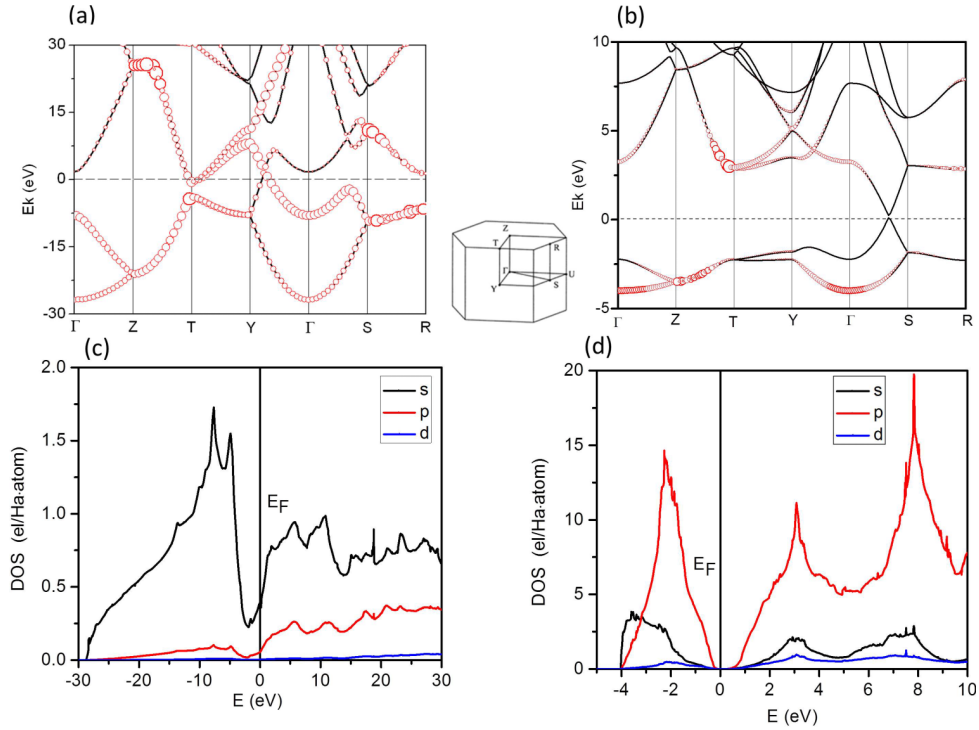

FIG. 6. ((a) and (c)) Same as Fig. 5, but for other directions. 1*s*- and 2*s*-characters of the wave functions are shown by red circles, for H and Li, respectively. ((b) and (d)) The corresponding density of states (DOS).

increased attraction also explains the higher value of the kinetic energy in *Cmca*-4 relative to *fcc*. These results are consistent with the previous conclusions that *Cmca*-4 is characterized by higher development of *s*-*p* electronic transition and a more pronounced localization of the valence charge density in the interstitial region.

The situation is completely different in hydrogen. Here, the last term in Eq. (4) is very small and the jump in $4PV$ can

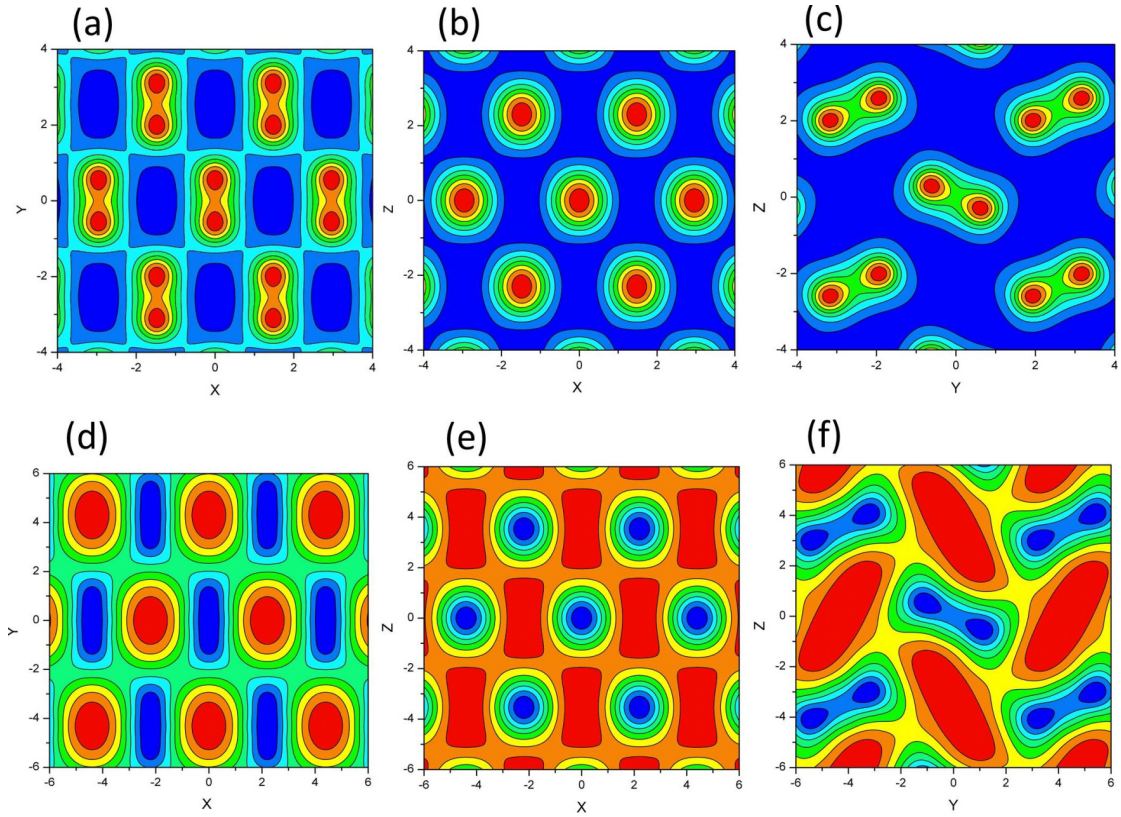

FIG. 7. Valence charge density in different cross sections for H ((a)–(c)) and Li ((c)–(e)) in the *Cmca*-4 structure. Hydrogen corresponds to $\Omega = 8.68$ bohrs^3 and 400 GPa, whereas Li to $\Omega = 33.51$ bohrs^3 and 130 GPa. ((a) and (d)) *xy* plane, ((b) and (e)) *xz* plane, and ((c) and (f)) *yz* plane.

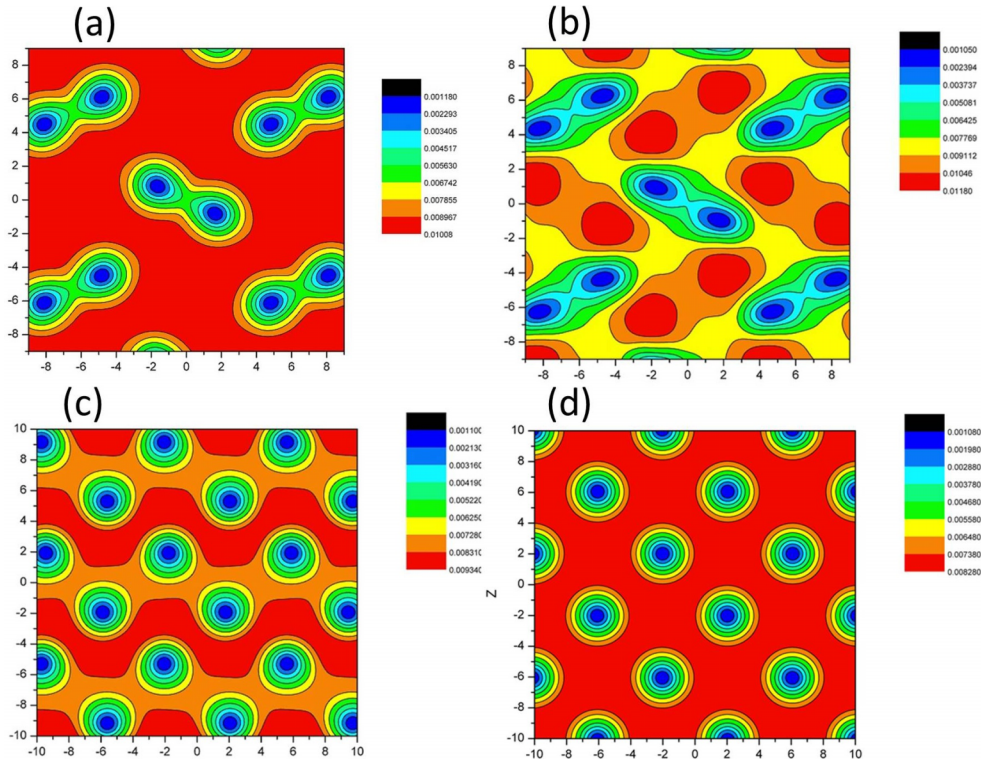

FIG. 8. Evolution of charge density in the yz plane as the structure changes from *Cmca*-4 to fcc in Li. (a) *Cmca*-4 corresponding to $\Omega = 113.10$ bohrs^3; the relative atomic positions are fixed to those with $\Omega = 33.51$ bohrs^3. (b) Structure obtained from (a) by relaxing the forces while keeping the lattice parameters the same. (c) Structure obtained from (b) by partial relaxation of both forces and stresses. (d) Fully relaxed structure (*fcc*) with $\Omega = 132.40$ bohrs^3.

TABLE II. Different contributions to the total energy E and enthalpy H per electron for hydrogen and uni-valent lithium in the *Cmca*-4 and *fcc* phases. For each element, the results for *Cmca*-4 are compared with two *fcc*'s at the same atomic volume and pressure. We also present r_s—the standard linear measure of average valence electronic density, $4\pi r_s^3/3 = \Omega$.

System	Hydrogen			Lithium		
Structure	*Cmca*-4	*fcc* (same Ω)	*fcc* (same P)	*Cmca*-4	*fcc* (same Ω)	*fcc* (same P)
Pressure (GPa)	300	241	300	130	183	130
Ω (bohrs^3)	9.738	9.738	9.100	33.510	33.510	38.576
r_s (bohrs)	1.325	1.325	1.295	2.000	2.000	2.096
Kinetic energy	0.780	0.720	0.747	0.405	0.400	0.360
Hartree energy	0.022	0.005	0.005	0.004	0.002	0.002
XC energy	−0.420	−0.407	−0.415	−0.394	−0.394	−0.379
Ewald energy	−0.632	−0.676	−0.692	−0.427	−0.448	−0.427
Psp energy	−0.269	−0.153	−0.152	0.159	0.201	0.178
Total energy (E)	−0.519	−0.511	−0.505	−0.254	−0.240	−0.266
H = E + PΩ	−0.419	...	−0.412	−0.105	...	−0.096

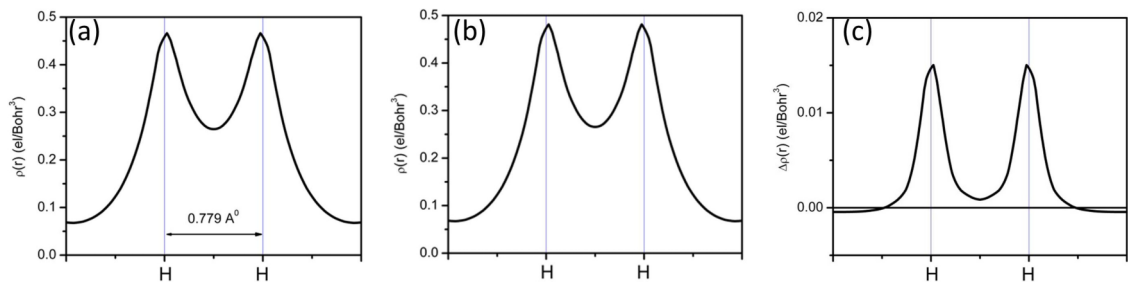

FIG. 9. Valence charge distribution along the line passing through the nearest protons in *Cmca*-4 H at 500 GPa calculated at two different cutoff radii r_c: (a) 0.5 bohrs and (b) 0.25 bohrs; (c) their difference.

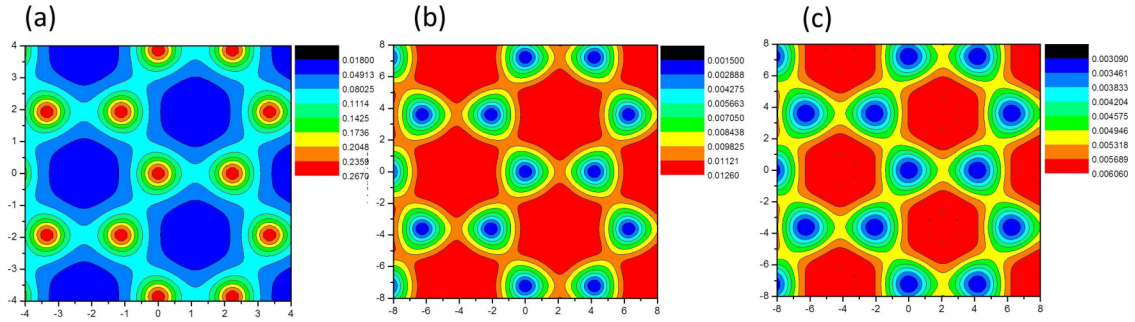

FIG. 10. Valence charge density for H and Li in the graphene structure. (a) H-graphene ($b = 2.09$ bohrs) and ((b) and (c)) Li-graphene ($b = 4.18$ bohrs); b is the nearest-neighbor distance. (a) and (b) in the $z = 0$ plane and (c) in $z = 2$ plane.

be compensated only by the jump in the sum,

$$-E_{kin} + \int \rho(\mathbf{r})(4\varepsilon_{xc} - 3\mu_{xc})d\mathbf{r}. \quad (5)$$

The further simplification comes from the fact that for the pressure ranges of interest, the second term of Eq. (5) in H is lower than in Li by an order of magnitude. Moreover, this term only slightly depends on structure and exhibits a negligible jump at a transition pressure. The minor role of the $\int \rho(\mathbf{r})(4\varepsilon_{xc} - 3\mu_{xc})\,d\mathbf{r}$ in H in comparison with Li can be easily understood. In H, the valence electron densities of interest are significantly higher than in Li (correspond to lower Wigner-Seitz radii r_s). We recall that in the $r_s \to 0$ limit (infinite density), the exchange effects dominate over correlations and the simple Slater X_α form for the exchange correlation energy ($\varepsilon_{xc} \sim \rho^{1/3}$) becomes progressively more accurate; also, in the X_α approach, $\varepsilon_{xc} = 3/4\mu_x$ (Ref. 54) and the second term of Eq. (5) is zero. At the transition pressure P_c, the kinetic energy E_{kin} must therefore suffer a drop by $\sim|4P\Delta V|$. At the same time, the potential energy E_{pot} must increase by $\sim|5P\Delta V|$ in agreement with the thermodynamic relation $\Delta(E_{kin} + E_{pot}) = -P\Delta V$. We checked these results numerically for the *Pbcn* $\to$ *Cmca*-4 and *Pbcn* $\to C2/c$ transitions between candidate structures. Good agreement was found between the predictions and results obtained by this approach.

As mentioned above, the pseudopotential for H is constrained to be finite at the nucleus, leading to cuspless wave functions at the proton positions. In reality, however, the electrons move in the bare Coulomb field, and according to the Kato cusp theorem,[63] their wave function (charge density) must exhibit a cusp at the positions of protons. The question thus arises about the sensitivity of the results of these calculations on the cutoff radius r_c, beyond which the pseudopotential becomes equal to the Coulomb $1/r$, especially at higher pressures. To examine this question, we compared the electron charge density and other ground state properties calculated for H as a function of cutoff radius. Figure 9 shows the charge density distribution along the line passing the nearest protons *Cmca*-4 H at two distinctly different cutoff radii—0.5 and 0.25 bohrs. As seen from the figure, the pseudopotential with smaller r_c tends to keep more electrons in the immediate neighborhood, in accordance with expectations. The effect, however, is small and has a negligible effect on the calculated properties of interest here. For example, in going from 0.5 to 0.25 bohrs, the total energy, for example, changes by 0.01% and the pressure by 0.06%. This observation is consistent with the fact that the last term in Eq. (4) is relatively small, as mentioned before.

D. Graphene structure

Recently, we showed that the special stability of layered structures in compressed molecular hydrogen can be explained by closed-shell effects similar to aromaticity.[64] This result arises from the observation that the *s*-electrons in hydrogen play a role similar to the π-electrons in conventional aromatic systems such as benzene or graphene. It is therefore of interest to examine the valence charge density of H and Li in such hypothetical graphene structures, where such closed-shell effects play a role in stabilizing this 2D honeycomb configuration for H.[64] As found for other structures, the valence charge density distributions in H and Li tend to mirror each other: the minima in H correspond to maxima in Li and vice versa (Fig. 10). Comparing the pattern observed for other structures, the mirroring is most notable for this structure as well as *Cmca*-4 (Figs. 7 and 10). It is somewhat less obvious for *fcc*, which is why for this structure we present ELFs (Figs. 2 and 3) the actual electron densities, as the former are inverted with respect to each other more distinctly than the latter.

Further insight into the high-pressure behavior of Li is obtained by examination of the band structures calculated for this element in the ideal graphene structure at different nearest-neighbor separations r. The calculated equilibrium separation of 5.15 bohrs is only 8% shorter than the corresponding separation in bulk *bcc* Li (5.57). At this stage, Li is already in a semimetallic state where the valence and conduction bands do not cross each other as functions of **k** vector but overlap in energy. This contrasts with H-graphene where the valence and conduction bands touch each other at (Dirac) points.[20] The difference is due to strong *s*-*p* hybridization in Li leading to an energy gap for all **k**-points along the K-M line in the Brillouin zone (Fig. 11, center); this is an "inverted" bandgap because the *p*-states lie *lower* than *s*-states (by ~0.25 eV). As the interatomic distance decreases, the gap along K-M widens, e.g., becoming ~1.34 eV at $r = 4.18$ (Fig. 11, left). At this separation, we can see two Dirac points at K where the second and third bands from one side and fourth and fifth bands from the other cross each other in a linear fashion. The first two bands have *s*-character, whereas the second two have the character of p_z-orbitals: only these band pairs can form Dirac points at K in graphene structure.[20] Just below $r = 4.18$, the global energy gap opens and the system enters

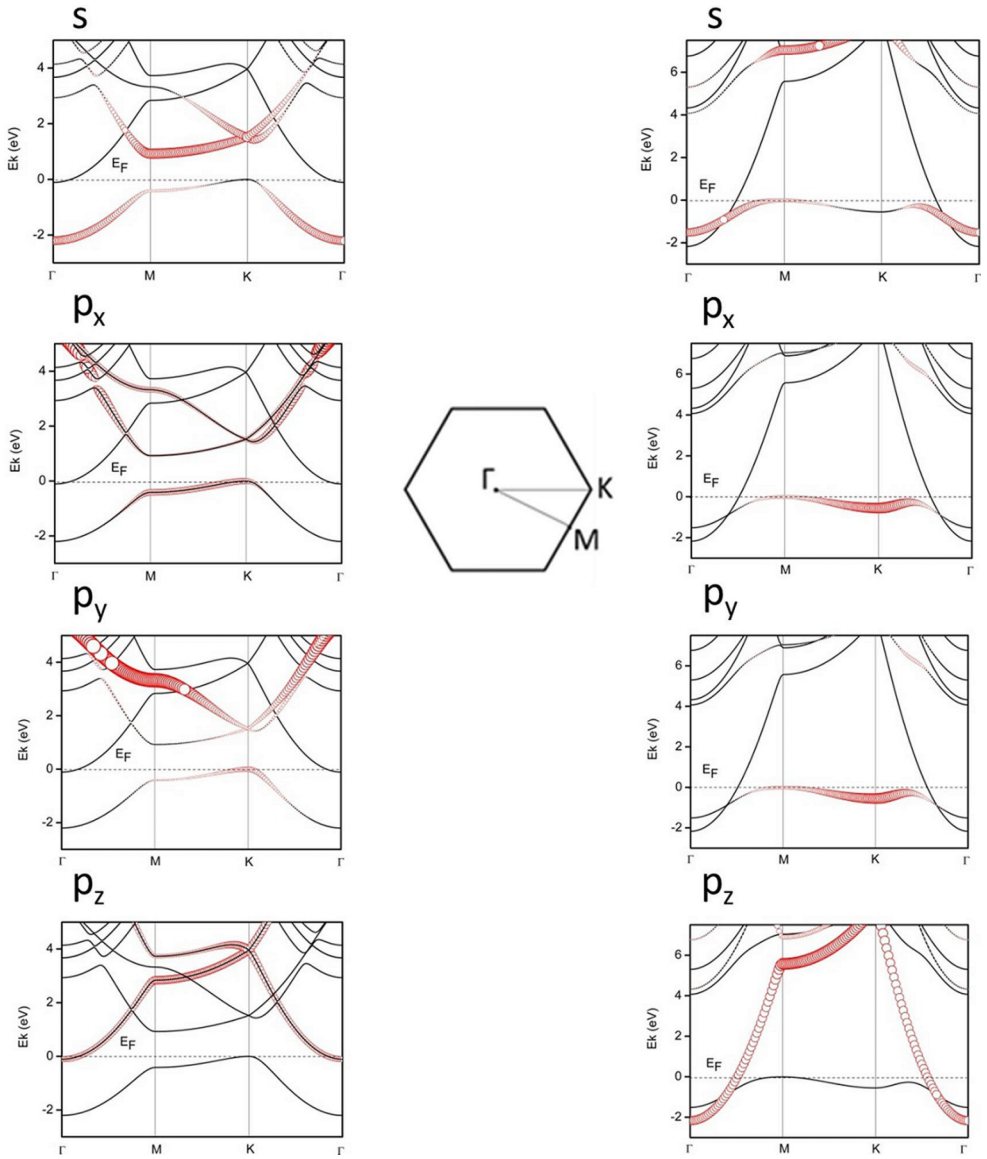

FIG. 11. Band structure of Li in the graphene structure at $r = 4.18$ bohrs (left column) and $r = 2.65$ bohrs (right column). The size of red circles is proportional to the character of corresponding wave functions.

a semiconducting state with an indirect gap. As the r further decreases, the hybridization gap along K-M quickly widens and at $r = 2.65$, it reaches a value of ~7 eV at the K point and somewhat less at the M point (Fig. 11, right). At the same time, the *sp*-hybrid bandwidth diminishes and the $2p_z$ band drops below the Fermi energy and even becomes the lowest in energy near the Γ-point. Such an evolution of the electronic spectrum with decreasing interatomic spacing corresponds to a "metal-dielectric-metal" sequence of transitions, mimicking that observed in 3D Li.

We should stress that despite the differences in their electronic structures, planar graphene-like structures are stabilized at high pressures for both Li and H. The special stability of these structures is associated with the completely (or *almost* completely) filled set of bonding orbitals or valence bands. In the case of H, such bonds are 1*s*-derived, whereas in Li, they have the character of *s*-*p* bonding orbitals. In going from 2D sheets to 3D compressed layered structures, the interaction between the sheets can further "dielectrize" the energy spectrum and reduce the kinetic energy. This additional stabilization, however, should be considered as a secondary to that existing already on the level of separate sheets.

IV. CONCLUSIONS

A detailed study of the chemical bonding in polymorphs of H and Li reveals insights into the similarities and differences in behavior of the lightest alkalis in the periodic table over a broad range of compressions. In particular, theoretical calculations of the bonding, electronic structure, and energetics are carried out and compared for the two elements in close-packed metallic, open covalent-like low-coordinated, and two-dimensional graphene structures. The two elements are found to exhibit strikingly different valence charge density distributions for the same arrangement of atoms. These distributions are in fact inverted with respect to each other: the minima in H correspond to maxima in Li and vice versa. Application of the virial theorem to these materials predicts that the jumps in

the kinetic and potential energies across the first-order phase transitions in them are opposite in sign.

Both elements undergo a continuous *s*-*p* electronic transition, which, however, is in a much earlier stage of development in Li because of the larger separation between the valence (1*s*) and higher energy (2*s* and 2*p*) levels in H. Despite this fact, the electronic transition is still able to induce an insulator-to-(semi)metal transition in the latter as a result of lowering of the 2*p*-derived band and its overlap with the 1*s* band. In contrast, in Li core, orthogonality effects and valence band splitting into bonding and antibonding *sp*-hybridized states across the Fermi level lead to the formation of a hybridization pseudogap and charge accumulation in the interstitial regions. Such an accumulation and its consequence—a partial or full dielectrization of the electronic spectrum—are in fact the manifestations of the strong *s*-*p* hybridization of such bands when the effective 2*p* and 2*s* atomic levels cross one another.[65] The Group 1 elements are now observed to exist as metals, insulators, and at the borderline of semiconducting-semimetallic states. Rather than textbook examples of the free-electron metals during compression, the alkalis should be considered textbook examples of a more general chemical picture of bonding in elemental solids.

ACKNOWLEDGMENTS

This research was supported by EFree, an Energy Frontier Research Center funded by the U.S. Department of Energy, Office of Science, Basic Energy Sciences under Award No. DE-SC-0001057. The infrastructure and facilities used are supported by U.S. National Science Foundation (No. DMR-1106132) and the U.S. Department of Energy/National Nuclear Security Administration (No. DE NA-00006, CDAC).

[1]E. Wigner and F. Seitz, Phys. Rev. **43**, 804 (1933).
[2]E. Wigner and H. B. Huntington, J. Chem. Phys. **3**, 764–770 (1935).
[3]R. T. Howie, C. L. Guillaume, T. Scheler, A. F. Goncharov, and E. Gregoryanz, Phys. Rev. Lett. **108**(12), 125501 (2012).
[4]M. I. Eremets and I. A. Troyan, Nat. Mater. **10**(12), 927–931 (2011).
[5]C. S. Zha, Z. Liu, M. Ahart, R. Boehler, and R. J. Hemley, Phys. Rev. Lett. **110**(21), 217402 (2013).
[6]P. Loubeyre, F. Occelli, and P. Dumas, Phys. Rev. B **87**(13), 134101 (2013).
[7]C. J. Pickard and R. J. Needs, Nat. Phys. **3**, 473 (2007).
[8]C. J. Pickard, M. Martinez-Canales, and R. J. Needs, Phys. Rev. B **85**, 214114 (2012).
[9]C. S. Zha, Z. Liu, and R. J. Hemley, Phys. Rev. Lett. **108**, 146402 (2012).
[10]B. Rousseau and N. W. Ashcroft, Phys. Rev. Lett. **101**, 046407 (2008).
[11]C. J. Pickard and R. J. Needs, Phys. Rev. Lett. **102**, 146401 (2009).
[12]M. Hanfland, R. J. Hemley, and H. K. Mao, Phys. Rev. Lett. **70**, 3760–3763 (1993).
[13]C. L. Guillaume, E. Gregoryanz, O. Degtyareva, M. I. McMahon, S. Evans, M. Hanfland, M. Guthrie, S. V. Sinogeikin, and H. K. Mao, Nat. Phys. **7**, 211–214 (2011).
[14]F. Datchi, P. Loubeyre, and R. LeToullec, Phys. Rev. B **61**, 6535–6546 (2000).
[15]E. Gregoryanz, A. F. Goncharov, K. Matsuishi, H. Mao, and R. J. Hemley, Phys. Rev. Lett. **90**, 175701 (2003).
[16]S. Deemyad and I. F. Silvera, Phys. Rev. Lett. **100**, 155701 (2008).
[17]M. I. Eremets and I. A. Troyan, JETP Lett. **89**, 198–203 (2009).
[18]Y. Feng, J. Chen, D. Alfè, X. Z. Li, and E. Wang, J. Chem. Phys. **142**, 064506 (2015).
[19]J. Chen, X. Z. Li, Q. Zhang, M. I. J. Probert, C. J. Pickard, R. J. Needs, A. Michaelides, and E. Wang, Nature Commun. **4**, 2064 (2013).
[20]I. I. Naumov, R. E. Cohen, and R. J. Hemley, Phys. Rev. B **88**, 045125 (2013).
[21]J. B. Neaton and N. W. Ashcroft, Nature **400**, 141–144 (1999).
[22]N. W. Ashcroft, J. Phys.: Condens. Matter **16**, S945–S952 (2004).
[23]M. Cohen and V. Heine, in *Solid State Physics: Advances and Applications*, edited by H. Ehrenreich, F. Seitz, and D. Turnbull (Academic Press, New York, 1970), Vol. 24, p. 38.
[24]V. Heine, in *Solid State Physics: Advances Applications*, edited by H. Ehrenreich, F. Seitz, and D. Turnbull (Academic Press, New York, 1970), Vol. 24, p. 1.
[25]V. Heine and D. Weaire, in *Solid State Physics: Advances and Applications*, edited by H. Ehrenreich, F. Seitz, and D. Turnbull (Academic Press, New York, 1970), Vol. 24, p. 250.
[26]Y. Ma, M. Eremets, A. P. Oganov, Y. Xie, I. Trojan, S. Medvedev, A. O. Lyakhov, M. Valle, and V. Prakapenka, Nature **458**, 182–185 (2009).
[27]T. Matsuoka, M. Sakata, Y. Nakamoto, K. Takahama, K. Ichimaru, K. Mukai, K. Ohta, N. Hirao, Y. Ohishi, and K. Shimizu, Phys. Rev. B **89**, 144103 (2014).
[28]T. Matsuoka and K. Shimizu, Nature **458**, 186–189 (2009).
[29]E. G. Maksimov, M. V. Magnitskaya, and V. E. Fortov, Phys.-Usp. **48**, 761–780 (2005).
[30]M. I. McMahon and R. J. Nelmes, Chem. Soc. Rev. **35**, 943–963 (2006).
[31]V. F. Degtyareva, Phys.-Usp. **49**, 369–388 (2006).
[32]V. F. Degtyareva, High Pressure Res. **30**, 343–371 (2010).
[33]V. E. Fortov and V. B. Mintsev, Russ. Chem. Rev. **82**, 597–615 (2013).
[34]B. Rousseau, Y. Xie, Y. Ma, and A. Bergara, Eur. Phys. J. B **81**, 1–14 (2011).
[35]M. S. Miao and R. Hoffmann, Acc. Chem. Res. **47**, 1311–1317 (2014).
[36]H. G. von Schnering and R. Nesper, Angew. Chemie, Int. Ed. **26**, 1059–1080 (1987).
[37]J. B. Neaton and N. W. Ashcroft, Phys. Rev. Lett. **86**, 2830–2833 (2001).
[38]U. Schwarz, O. Jepsen, and K. Syassen, Solid State Commun. **113**, 643–648 (2000).
[39]M. Hanfland, K. Syassen, N. E. Christensen, and D. L. Novikov, Nature **408**, 174 (2000).
[40]B. Rousseau, K. Uehara, D. D. Klug, and J. S. Tse, ChemPhysChem **6**, 1703 (2005).
[41]M. Marques, M. I. McMahon, E. Gregoryanz, M. Hanfland, C. L. Guillaume, C. J. Pickard, G. J. Ackland, and R. J. Nelmes, Phys. Rev. Lett. **106**, 095502 (2011).
[42]E. Zurek, O. Jepsen, and O. K. Andersen, ChemPhysChem **6**, 1934 (2005).
[43]J. L. Dye, Nature **365**, 10 (1993).
[44]J. L. Dye, M. J. Wagner, G. Overney, R. H. Huang, T. F. Nagy, and D. Tomanek, J. Am. Chem. Soc. **118**, 7329–7336 (1996).
[45]D. J. Singh, H. Krakauer, C. Haas, and W. E. Pickett, Nature **365**, 39–42 (1993).
[46]R. Rencsok, T. A. Kaplan, and J. F. Harrison, J. Chem. Phys. **98**, 9758–9764 (1993).
[47]R. Rousseau and D. Marx, Chem. Euro. J. **6**, 2982–2993 (2000).
[48]A. M. Pendas, M. A. Blanco, A. Costales, P. M. Sanchez, and V. Luana, Phys. Rev. Lett. **83**, 1930–1933 (1999).
[49]Y. Yao, J. S. Tse, and D. D. Klug, Phys. Rev. Lett. **102**, 115503 (2009).
[50]I. I. Naumov and R. J. Hemley, Phys. Rev. Lett. **114**, 156403 (2015).
[51]A. F. Goncharov, J. S. Tse, H. Wang, J. Yang, V. V. Struzhkin, R. T. Howie, and E. Gregoryanz, Phys. Rev. B **87**, 024101 (2013).
[52]J. Ihm, A. Zunger, and M. Cohen, J. Phys. C: Solid State Phys. **12**, 4409 (1979).
[53]A. P. P. Natalense, C. S. Sartori, L. G. Ferreira, and M. A. P. Lima, Phys. Rev. A **54**, 5436 (1996).
[54]M. T. Yin, Phys. Rev. B **27**, 7769 (1983).
[55]M. H. McAdon and W. A. Goddard III, Phys. Rev. Lett. **55**, 2563–2566 (1985).
[56]M. H. McAdon and W. A. Goddard III, J. Phys. Chem. **91**, 2607–2626 (1987).
[57]U. Häussermann and S. I. Simak, Phys. Rev. B **64**, 245114 (2001).
[58]N. W. Ashcroft and N. D. Mermin, *Solid State Physics*, 1st ed. (Saunders College, Philadelphia, PA, 1976).
[59]N. W. Ashcroft, J. Phys. C.: Solid State Phys. **1**, 232 (1968).
[60]M. B. Lepetit, E. Apra, J. P. Malrieu, and R. Dovesi, Phys. Rev. B **46**, 12974 (1992).
[61]J. C. Boettger and S. B. Trickey, Phys. Rev. B **32**, 3391 (1986).
[62]B. Edwards and N. W. Ashcroft, Nature **388**, 652–655 (1997).
[63]T. Kato, Commun. Pure Appl. Math. **10**, 151–177 (1957).
[64]I. I. Naumov and R. J. Hemley, Acc. Chem. Res. **47**, 3551–3559 (2014).
[65]A. K. McMahan, Physica B+C **139-140**, 31–41 (1986).